High-pressure synthesis and structural, transport, and magnetic properties of rutile-type Cr_2ReO_6 and $CrReO_4$

Y. Y. Jiao,[1,2] Q. Cui,[1,2] P. Shahi,[1,2] N. N. Wang,[1,2] N. Su,[1,2] B. S. Wang,[1,2] M. T. Fernández-Díaz,[3] J. A. Alonso,[4,*] and J.-G. Cheng[1,2,†]

[1]*Beijing National Laboratory for Condensed Matter Physics and Institute of Physics, Chinese Academy of Sciences, Beijing 100190, China*

[2]*School of Physical Sciences, University of Chinese Academy of Sciences, Beijing 100190, China*

[3]*Institut Laue Langevin, BP 156X, Grenoble F-38042, France*

[4]*Instituto de Ciencia de Materiales de Madrid, CSIC, Cantoblanco, E-28049 Madrid, Spain*

(Received 6 November 2017; published 22 January 2018)

We have synthesized the cation ordered rutile-type Cr_2ReO_6 and $CrReO_4$ under high-pressure and high-temperature conditions and performed detailed characterizations on their structural, transport, and magnetic properties via x-ray and neutron powder diffraction, resistivity, magnetic susceptibility, and specific heat measurements. Cr_2ReO_6 crystallizes in the inverse trirutile structure with lattice parameters $a = b = 4.552\,21(5)$ Å and $c = 8.8934(1)$ Å in the space group $P4_2/mnm$. It undergoes a second-order antiferromagnetic transition at $T_N \approx 67$ K with the magnetic structure described by the propagation vector $\mathbf{k} = [0.5,0,0.5]$. For $CrReO_4$, it adopts a monoclinically distorted rutile-like structure with unit-cell parameters $a = 9.3393(2)$ Å, $b = 5.6869(1)$ Å, $c = 4.6243(1)$ Å, and $\beta = 92.043(8)^\circ$ in the space group $C2/m$. It also exhibits an antiferromagnetic order at $T_N = 98$ K with the magnetic structure described by the propagation vector $\mathbf{k} = [1,0,0.5]$. Interestingly, a large paramagnetic Weiss temperature of $\theta_{CW} = -478$ K is evidenced from the Curie-Weiss fitting to the inverse magnetic susceptibility. The temperature dependence of resistivity $\rho(T)$ for both compounds can be described with Mott's variable range hopping mechanism in the one-dimensional model for Cr_2ReO_6 and the three-dimensional model for $CrReO_4$, respectively. For both compounds, a weak resistivity anomaly can be discerned around T_N from the temperature derivative curves, signaling the interplay of charge and spin degrees of freedom for these $3d$(Cr)-$5d$(Re) coupled electron systems.

DOI: 10.1103/PhysRevB.97.014426

I. INTRODUCTION

Complex transition-metal oxides with cation ordering are of particular interest because the periodic arrangement of different electronic configurations offers additional degrees of freedom to tune the physical properties [1–3]. For a given structure, the cation ordering usually takes place at certain compositions for combinations of different charge valence states; the larger difference in the charge valences or the cation sizes, the stronger tendency for cation ordering [4]. For the simple AO_2 rutile structure, some derivatives with an ordered arrangement of cations can be formed in the mixed oxides $A_{1-x}B_xO_2$. As illustrated in Fig. 1, the cation-ordered inverse trirutile structure A_2BO_6 and monoclinically distorted "birutile" ABO_4 can be adopted for $x = 1/3$ and $1/2$, respectively. For example, these structure-related variants have been observed in the Cr-based mixed oxides $Cr_{1-x}B_xO_2$, including the inverse trirutile $Cr^{3+}{}_2B^{6+}O_6$ (B = Mo, W, Te) [5–7] and the monoclinically distorted birutile $Cr^{3+}B^{5+}O_4$ (B = Mo, W) [8,9]. These Cr-based inverse trirutile compounds display distinct magnetic structures due to the different d-shell occupancy of the counter B^{6+} cations [6,10,11], which are used to maintain the charge neutrality, whereas the birutile compounds are featured by B^{5+}-B^{5+} pairs with metallic bonding [8]. Since the counter B cation with partially filled d orbitals can bring different magnetic interactions and orbital hybridizations, it is thus interesting to investigate more cation ordered rutile-type compounds.

Cr_2ReO_6 with $Re^{6+}(5d^1)$ is such a candidate material. It was synthesized by Sleight in 1975 under high-pressure and high-temperature (HPHT) conditions, but no detailed structural and physical properties were reported [12]. Later on, Mikhailova *et al.* [13] investigated the mixed chromium-rhenium oxides $Cr_{1-x}Re_xO_2$ in the composition range $0.33 \leqslant x \leqslant 0.69$. Since the rhenium oxides are easily oxidized to volatile Re_2O_7 upon heating in air, these samples were synthesized either in evacuated sealed silica tubes or under HPHT conditions. For the syntheses in a sealed silica tube, only the compositions $Cr_{1-x}Re_xO_2$ in the range $0.56 \leqslant x \leqslant 0.69$ can be obtained as a nearly single phase of simple rutile structure with a random cation distribution, Fig. 1(a); the unit cell is tetragonal with lattice constants $a \approx 4.7$ Å and $c \approx 2.8$ Å. For the synthesis at 5 GPa and 1350 °C, $Cr_{1-x}Re_xO_2$ with $x \approx 0.5$ were also obtained as a simple rutile structure without cation ordering. When increasing the synthesis pressure to 9 GPa for the initial composition "$Cr_{0.67}Re_{0.33}O_2$," the resultant product contains three phases, i.e., the monoclinic birutile phase (space group $C2/m$), Cr_2O_3 and ReO_2. After three months, the monoclinic

*ja.alonso@icmm.csic.es
†jgcheng@iphy.ac.cn

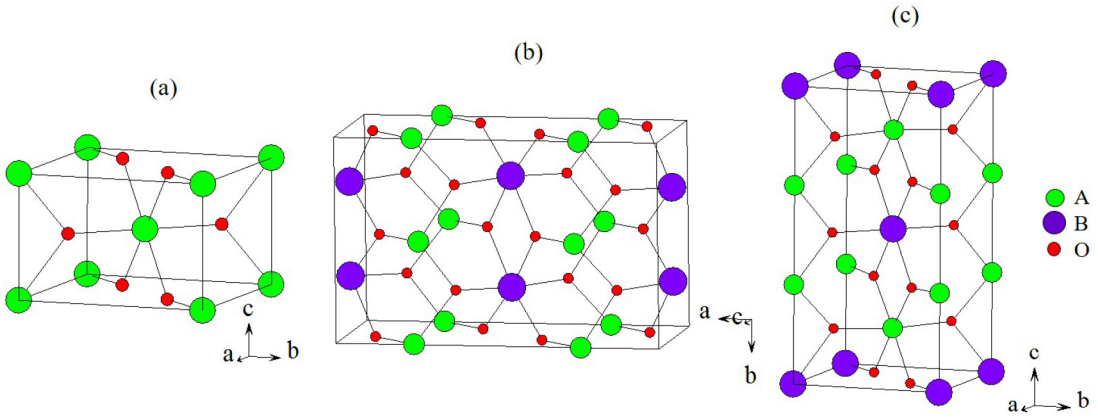

FIG. 1. Schematic drawing of the crystal structures for (a) the simple rutile AO_2, (b) the monoclinically distorted "birutile" ABO_4, and (c) the inverse trirutile A_2BO_6. The crystal structures of these rutile-type derivatives are featured by edge-shared A/BO_6 octahedral chains along the c axis for the simple rutile (a) and the inverse trirutile (c), or along the b axis for the "birutile" (b).

phase was found partially transformed to Cr_2ReO_6 with a trirutile structure (space group $P4_2/mnm$). The crystal structures of the monoclinic birutile $CrReO_4$ and the tetragonal trirutile Cr_2ReO_6 have been refined from the powder x-ray diffraction data of the mixed-phase sample in Ref. [13]. However, the physical properties of these cation-ordered compounds were not reported due to the multiple-phase nature. The purpose of the present study is to fill the knowledge gap by characterizing the physical properties of these cation-ordered rutile-type compounds with partially filled $5d$ orbitals.

In this work, we have successfully obtained nearly single-phase Cr_2ReO_6 and $CrReO_4$ under moderate HPHT conditions and characterized their electrical transport and magnetic properties. We found that the optimal synthesis conditions are 6 GPa, 1000 °C for Cr_2ReO_6, and 4 GPa, 1000 °C for $CrReO_4$, respectively. Both compounds are found to undergo a second-order antiferromagnetic (AF) transition at $T_N \approx 67$ K and 98 K, respectively. Their magnetic structures were determined via analysis of the neutron powder diffraction patterns. In addition, both compounds exhibit a semiconducting behavior in the investigated temperature range 2–300 K; their temperature dependences of resistivity $\rho(T)$ can be described by Mott's variable range hopping (VRH) mechanism in the one-dimensional model for Cr_2ReO_6 and in the three-dimensional model for $CrReO_4$, respectively. For both compounds, a weak resistivity anomaly can be discerned around T_N from the temperature derivative curves, signaling the interplay of charge and spin degrees of freedom for these $3d-5d$ coupled systems.

II. EXPERIMENT

All HPHT syntheses in the present study were performed with a Kawai-type multianvil module (Max Voggenreiter GmbH) in the Institute of Physics, CAS. A semi-sintered octahedron made of Ceramacast 584-OF is used as the pressure transmitting medium, and the graphite sleeve serves as a heater. The samples are contained in the Au capsule. For the synthesis of Cr_2ReO_6, a stoichiometric mixture of Cr_2O_3 and ReO_3 powders was subjected to heat treatment at 6 GPa and 1000 °C for 30 min. For $CrReO_4$, the starting materials are Cr_2O_3, ReO_3, and Re powders mixed in the ratio of 6:11:1, and were reacted at 4 GPa and 1000 °C for 30 min. For each synthesis, the temperature was quenched to room temperature before releasing pressure slowly. The sample was finally recovered and subjected to various measurements of physical properties at ambient pressure.

Phase purity of the obtained Cr_2ReO_6 and $CrReO_4$ polycrystalline samples were first examined by powder x-ray diffraction (XRD) at room temperature. In order to extract reliable structural parameters and to determine the magnetic structure, we also performed neutron powder diffraction (NPD) at the Institut Laue Langevin, Grenoble, on Cr_2ReO_6 and $CrReO_4$ gathered from more than ten batches of samples synthesized under similar conditions. For the structural refinements, NPD experiments were carried out at room temperature in the high-resolution powder diffractometer D2B ($\lambda = 1.594$ Å). To resolve the magnetic structures, NPD patterns were collected at 2 K for Cr_2ReO_6 and at 2 and 120 K for $CrReO_4$ in the high-flux diffractometer D20 with a longer wavelength ($\lambda = 2.41$ Å). The powder samples were contained in vanadium cylinders; and a time of 2 h was required to collect the full diffraction pattern given the small available sample. The NPD data were analyzed with the Rietveld method [14] by using the FULLPROF program [15]. A pseudo-Voigt function was chosen to generate the line shape of the diffraction peaks. The following parameters were refined in the final run: scale factor, background coefficients, zero-point error, pseudo-Voigt corrected for asymmetry parameters, positional coordinates and isotropic thermal factors for all the atoms, as well as the magnetic moments for the magnetic structures. The neutron scattering lengths for Cr, Re, and O are 3.635, 9.20, and 5.803 fm, respectively.

DC magnetic susceptibility was measured with a commercial magnetic property measurement system (MPMS-III, Quantum Design) in the temperature range 2–300 K under an external magnetic field of $\mu_0 H = 1$ T. Isothermal magnetization $M(H)$ curves were recorded in the field range $+7\,\text{T} \sim -7\,\text{T}$. Specific heat and resistivity in the temperature range 2–300 K were collected by the physical property measurement system (PPMS, Quantum Design).

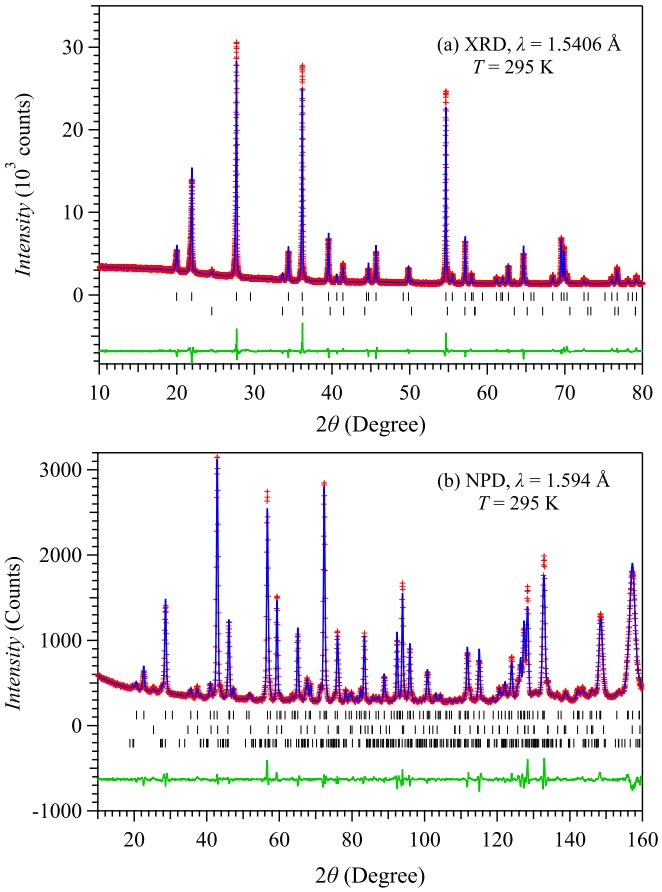

FIG. 2. Observed (cross), calculated (line), and their difference (bottom line) profiles for (a) XRD and (b) NPD of Cr_2ReO_6 after Rietveld refinements. The first and second row of tick marks in (a) represent the Bragg positions of the trirutile Cr_2ReO_6 and the impurity Cr_2O_3, respectively. The tick marks in (b) represent the Bragg positions of the trirutile Cr_2ReO_6, Cr_2O_3, and the monoclinic $CrReO_4$, respectively.

III. RESULTS AND DISCUSSION

A. Cr_2ReO_6

Figure 2(a) shows the powder XRD pattern of Cr_2ReO_6 prepared at 6 GPa and 1000 °C. It confirms that the as-obtained sample is nearly single phase with inverse trirutile structure and contains a small amount of Cr_2O_3 impurity. In order to extract reliable structural parameters, especially the oxygen positional parameters, we have synthesized more than ten batches of samples under similar conditions for NPD measurement. It turns out that in addition to Cr_2O_3 the NPD pattern also contains some monoclinic $CrReO_4$ phase. This is presumably because the stability range of Cr_2ReO_6 is rather narrow and some batches contain $CrReO_4$. But this should not influence the structural analysis. Finally, the obtained NPD pattern was refined by including these three phases. The inverse trirutile structure of Cr_2ReO_6 is defined in the space group $P4_2/mnm$ (no. 136) with the Re atom at 2*a* (0, 0, 0), the Cr atom at 4*e* (0, 0, z), and two kinds of O atoms at 4*f* (*x*, *x*, 0) and 8*j* (*x*, *x*, *z*) positions, respectively. The structural models for Cr_2O_3 with rhombohedral space group *R*-3*c* and $CrReO_4$ with monoclinic *C*2/*m* space group are taken from the literature [13]. The refinement converged well as illustrated in Fig. 2(b). The obtained atomic parameters, the main interatomic distances and angles for Cr_2ReO_6 after refinements are listed in Tables I and II. Rietveld refinements allowing the Cr/Re site exchange indicated a high degree of cation ordering with the cation site mixing less than 4%. This should be attributed to the large difference of the valence states for Cr^{3+} and Re^{6+} ions.

The obtained lattice parameters $a = 4.552\,21(5)$ Å and $c = 8.8934(1)$ Å are close to those reported by Sleight [12] of $a = 4.551$ Å, $c = 8.907$ Å, and by Mikhaliova *et al.* [13] of $a = 4.5420(1)$ Å, $c = 8.9173(4)$ Å. From the scale factors, the amounts of Cr_2O_3 and $CrReO_4$ are estimated to be ~6.6 and 11 wt%, respectively. As depicted in Fig. 1(c), the crystal structure of Cr_2ReO_6 consists of parallel columns of edge-shared $[Cr_2ReO_{14}]_\infty$ octahedral chain extending along the *c* axis. The nearest-neighbor Cr-Cr and Cr-Re distances within the chains are 3.026(2) and 2.934(4) Å, respectively. These columns are connected with each other through corner-shared oxygen atoms. As seen in Table II, there are three sets of Cr-O distances for the CrO_6 octahedron, with an average distance

TABLE I. Atomic coordinates and isotropic thermal factors B_{iso}[Å^2] for Cr_2ReO_6 from powder NPD data[a] at 295 K. Space group $P4_2/mnm$ (no. 136), $a = b = 4.55221(5)$ Å, $c = 8.893\,41(12)$ Å, $V = 184.295(4)$ Å^3, $Z = 2$.

Atom	site	*x*	*y*	*z*	B_{iso}
Cr	4e	0.0	0.0	0.3299(5)	0.03(5)
Re	2a	0.0	0.0	0.0	0.58(5)
O1	8j	0.3029(3)	0.3029(3)	0.3364(5)	0.66(4)
O2	4f	0.2999(3)	0.3029(3)	0.0	0.90(8)

[a]Discrepancy factors: $R_p = 2.99\%$, $R_{wp} = 4.01\%$, $R_{exp} = 1.77\%$, $\chi^2 = 5.14$, $R_{Bragg} = 3.56\%$.

TABLE II. Main interatomic distances (Å) and angles (°) of Cr_2ReO_6 from powder NPD data at 295 K.

Bond length (Å)			
CrO_6 octahedron		ReO_6 octahedron	
Cr-O1	1.951(1)	Re-O1[a]	1.931(3)
Cr-O1[e]	1.951(1)	Re-O1[b]	1.931(3)
Cr-O1[a]	1.949(4)	Re-O1[c]	1.931(3)
Cr-O1[b]	1.949(4)	Re-O1[d]	1.931(3)
Cr-O2[f]	1.987(4)	Re-O2	1.931(2)
Cr-O2[b]	1.987(4)	Re-O2[e]	1.931(2)
⟨Cr-O⟩	1.962(3)	⟨Re-O⟩	1.931(2)
Cr-Cr[g]	3.026(2)	Cr-Re	2.934(4)
Bond angle (°)			
Cr[h]-O2-Cr[i]	99.2(1)	Re-O1-Cr	98.28(16)
Cr-O1-Cr[h]	128.93(8)	Re-O2-Cr[h]	130.4(2)
Cr[e]-O1-Cr[j]	128.93(8)	Re-O1-Cr	132.79(8)

Symmetry transformations used to generate equivalent atoms: [a]0.5−x, −0.5+y, 0.5−z; [b]−0.5+x, 0.5−y, 0.5−z; [c]0.5−y, −0.5+x, −0.5+z; [d]−0.5+y, 0.5−x, −0.5+z; [e]−x, −y, z; [f]0.5−y, −0.5+x, 0.5+z; [g]y, x, 1−z; [h]0.5+x, 0.5−y, 0.5−z; [i]0.5+y, 0.5−x, −0.5+z; [j]0.5−x, 0.5+y, 0.5−z.

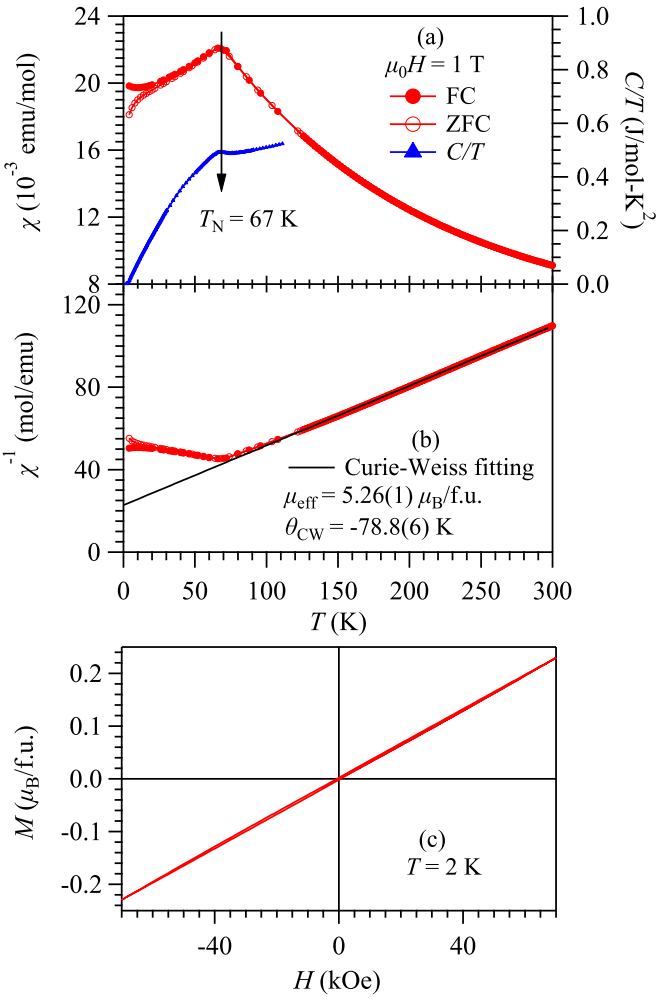

FIG. 3. (a) Temperature dependence of the magnetic susceptibility $\chi(T)$ and the specific heat divided by temperature C/T for Cr_2ReO_6. (b) Temperature dependence of the inverse susceptibility $\chi^{-1}(T)$ and the Curie-Weiss fitting curve shown by the solid line. (c) Field dependence of the isothermal magnetization $M(H)$ at 2 K.

of 1.962 Å shorter than the ionic radii sum for Cr^{3+} (0.615 Å) and O^{2-} (1.40 Å) [16]. The longest Cr-O2 bond connects with the nearest edge-shared Cr octahedron. On the other hand, the ReO_6 octahedron is regular with the same Re-O distances of 1.931(3) Å, which is also slightly smaller than the ionic radii sum for Re^{6+} (0.55 Å) and O^{2-} (1.40 Å). The Cr-O-Cr/Re bond angles are ∼100° within the edge-shared octahedral chain, and ∼130° in between the octahedral chains.

Figure 3(a) shows the temperature dependence of the dc magnetic susceptibility $\chi(T)$ for Cr_2ReO_6 measured upon warming up after zero-field cooled (ZFC) and field cooled (FC) from room temperature under an external magnetic field of $\mu_0 H = 1$ T. Both ZFC and FC $\chi(T)$ curves exhibit a cusp anomaly near $T_N = 67$ K, signaling the appearance of a long-range AF order. The observation of a specific-heat anomaly around T_N further confirms that the AF order is an intrinsic magnetic transition of Cr_2ReO_6. As seen in Fig. 3(b), the inverse susceptibility $\chi^{-1}(T)$ follows nicely the Curie-Weiss (CW) behavior in the paramagnetic region; a CW fitting to the $\chi^{-1}(T)$ in the temperature range 100–300 K yields an effective moment of $\mu_{eff} = 5.26(1)\mu_B$/f.u. and a CW temperature of $\theta_{cw} = -78.8(6)$ K. The obtained μ_{eff} is smaller than the expected value of $5.74\mu_B$/f.u. for the localized moments of Cr^{3+} ($g = 2$, $S = 3/2$) and Re^{6+} ($g = 2$, $S = 1/2$), presumably due to the reduced moment of Re^{6+} ion as confirmed by the NPD refinement below. The negative θ_{cw} signals dominant AF interaction in this compound. Figure 3(c) shows the isothermal $M(H)$ curve of Cr_2ReO_6 at 2 K, which exhibits a linear behavior in agreement with the AF order nature. The magnetization reaches only $0.22\mu_B$/f.u. at 7 T and 2 K.

To determine the magnetic structure below T_N, we collected a NPD pattern at 2 K in the high-flux D20 diffractometer and observed the appearance of some additional weak reflections of magnetic origin, which can be indexed with the propagation vector $\mathbf{k} = [0.5,0,0.5]$. The MAXMAGN application from the Bilbao Crystallographic Server was used to determine the magnetic structure [17]. Using the space group of the paramagnetic phase, i.e., the parent space group $P4_2/mnm$ (no. 136), and the propagation vector $\mathbf{k} = [0.5,0,0.5]$, we determined the possible magnetic space groups of maximal symmetry consistent with this propagation vector. Taking into account the site symmetry of the magnetic atoms in the paramagnetic structure, the program determines the spin arrangements and the refinable parameters for the magnetic moments for each one of the possible k-maximal symmetries.

After trying different possibilities, the best fit between observed and calculated magnetic reflections was found for the magnetic subgroup P_a2_1/c, with the magnetic moments shown in Table III for each atom in the magnetic unit cell. The good agreement between observed and calculated neutron profiles is shown in Fig. 4(a). The first and second reflection marks correspond to the Cr_2O_3 and $CrReO_4$ minor impurities, and the third row belongs to the crystal and magnetic structure of Cr_2ReO_6. The magnetic reflections are indicated by the arrows in the figure.

The determined magnetic structure for Cr_2ReO_6 is displayed in Fig. 4(b). It was found that the Cr moments lie in the bc plane and exhibit an AF arrangement along the a and c axes and a ferromagnetic alignment along the b axis. The refined magnitude of the Cr moment at 2 K is $1.63\mu_B$, smaller than the expected value for Cr^{3+} (t_{2g}^3) of $3\mu_B$. Concerning the Re magnetic moments, they exhibit a very small refined magnitude of $\sim 0.26\mu_B$, adopting a collinear arrangement approximately within the ac plane. Table IV gathers the magnitudes of the components of the Cr and Re magnetic moments.

The temperature dependence of resistivity $\rho(T)$ shown in Fig. 5 demonstrates a semiconducting behavior for Cr_2ReO_6; its resistivity at room temperature is 0.048 Ω cm and increases by more than six orders of magnitude upon cooling down to 2 K. In order to analyze its conduction mechanism, we have plotted the $\rho(T)$ data in various thermal activated formulas, and found that $\rho(T)$ can be best described by the Mott's VRH model for the one-dimensional system [18], i.e., $\rho = \rho_0 \exp(T/T_0)^{-1/2}$, in which T_0 is the activation energy. As seen in Fig. 5(b), the plot of $\ln\rho$ versus $T^{-1/2}$ produces nice linear regions above and below T_N, around which an inflection point can be defined from the derivative curve. The Mott's activation energy T_0 is estimated to be 3696(16) K for $T > T_N$ and 5072(37) K for $T < T_N$, respectively. Since $T_0 \propto [N(E_F)\xi]^{-1}$ for the one-dimensional system inversely proportional to the

TABLE III. Atomic positions, Wyckoff positions, and magnetic moments for Cr_2ReO_6 and $CrReO_4$ at 2 K from NPD data.

	N	Atom	New WP	Multiplicity	Magnetic moment
Cr_2ReO_6	1	Cr 0.00000 0.00000 0.16574	$(0,0,z \mid m_x,m_y,m_z)(1/4,1/2,z+1/4 \mid m_x,-m_y,m_z)$ $(1/4,1/2,-z+1/4 \mid m_x,-m_y,m_z)(0,0,-z \mid m_x,m_y,m_z)$ $(0,0,z+1/2 \mid -m_x,-m_y,-m_z)(1/4,1/2,z+3/4 \mid -m_x,m_y,-m_z)$ $(1/4,1/2,-z+3/4 \mid -m_x,m_y,-m_z)(0,0,-z+1/2 \mid -m_x,-m_y,-m_z)$ $(1/2,0,z \mid -m_x,-m_y,-m_z)(3/4,1/2,z+1/4 \mid -m_x,m_y,-m_z)$ $(3/4,1/2,-z+1/4 \mid -m_x,m_y,-m_z)(1/2,0,-z \mid -m_x-m_y,-m_z)$ $(1/2,0,z+1/2 \mid m_x,m_y,m_z)(3/4,1/2,-z+3/4 \mid m_x,-m_y,m_z)$ $(3/4,1/2,-z+3/4 \mid m_x,-m_y,m_z)(1/2,0,-z+1/2 \mid m_x,m_y,m_z)$	16	$(\mathbf{M_x},\mathbf{M_y},\mathbf{M_z})$
	2	Re 0.00000 0.00000 0.00000	$(0,0,0 \mid m_x,m_y,m_z)(1/4,1/2,1/4 \mid m_x,-m_y,m_z)$ $(0,0,1/2 \mid -m_x,-m_y,-m_z)(1/4,1/2,3/4 \mid -m_x,m_y,-m_z)$ $(1/2,0,0 \mid -m_x,-m_y,-m_z)(3/4,1/2,1/4 \mid -m_x,m_y,-m_z)$ $(1/2,0,1/2 \mid m_x,m_y,m_z)(3/4,1/2,3/4 \mid m_x,-m_y,m_z)$	8	$(\mathbf{M_x},\mathbf{M_y},\mathbf{M_z})$
$CrReO_4$	1	Cr 0.24827 0.00000 0.25070	$(x,0,z \mid m_x,0,m_z)(-x,0,-z \mid -m_x,0,-m_z)$ $(x+1/2,1/2,z \mid -m_x,0,-m_z)(-x+1/2,1/2,-z \mid m_x,0,m_z)$ $(x,0,z+1/2 \mid -m_x,0,-m_z)(-x,0,-z+1/2 \mid m_x,0,m_z)$ $(x+1/2,1/2,z+1/2 \mid m_x,0,m_z)(-x+1/2,1/2,-z+1/2 \mid -m_x,0,-m_z)$	8	$(\mathbf{M_x},\mathbf{0},\mathbf{M_z})$
	2	Re Re 0.00000 0.77668 0.00000	$(0,y,0 \mid 0,m_y,0)(0,-y,0 \mid 0,-m_y,0)$ $(1/2,y+1/2,0 \mid 0,-m_y,0)(1/2,-y+1/2,0+0,m_y,0)$ $(0,y,1/2 \mid 0,-m_y,0)(0,-y,1/2 \mid 0,m_y,0)$ $(1/2,y+1/2,1/2 \mid 0,m_y,0)(1/2,-y+1/2,1/2 \mid 0,-m_y,0)$	8	$(\mathbf{0},\mathbf{M_y},\mathbf{0})$

density of states at Fermi level $N(E_F)$ and the localization length ξ, the increase of T_0 below T_N should be ascribed to the decrease of $N(E_F)$ or ξ due to the development of AF order.

B. $CrReO_4$

Figure 6(a) shows the XRD pattern of the $CrReO_4$ sample prepared at 4 GPa and 1000 °C. It confirms that the as-obtained sample is single phase with the monoclinic birutile structure. We have refined the crystal structure in the monoclinic $CrWO_4$ structural model [9] defined in the space group $C2/m$ (no. 12) with the Cr atom at $4i$ $(x, 0, z)$, the Re atom at $4h$ $(0, y, 1/2)$, and three kinds of O atoms at $4i$ and $8j$ sites, respectively. We also collected a NPD pattern at 120 K and performed Rietveld refinement to extract more reliable structural parameters. The goodness of fitting is illustrated in Fig. 6(b). The obtained atomic parameters, the main interatomic distances and angles for $CrReO_4$ at 295 K (XRD) and 120 K (NPD) are listed in Tables V and VI. The obtained unit-cell parameters at 295 K are $a = 9.3283(2)$ Å, $b = 5.6870(1)$ Å, $c = 4.6228(1)$ Å, and $\beta = 92.065(7)°$, which are close to those reported by Mikhaliova *et al.* [13].

As depicted in Fig. 1(b), the crystal structure of $CrReO_4$ consists of parallel columns of edge-shared $[CrO_6]_\infty$ and $[ReO_6]_\infty$ octahedral chains extending along the b axis; these chains are connected with each other via corner-shared oxygens. The nearest-neighbor Cr-Cr distance within the $[CrO_6]_\infty$ chain is uniform and equals to 2.846(2) Å, whereas the $[ReO_6]_\infty$ chains contain alternative short and long nearest-neighbor Re-Re distances of 2.565(2) Å and 3.122(2) Å, respectively. The short Re-Re distance is even shorter than that in the Re metal, signaling the formation of Re-Re pair with metallic bonding. A similar situation has also been observed in $CrMoO_4$ [8]. In contrast with Cr_2ReO_6, both CrO_6 and ReO_6 octahedron in $CrReO_4$ exhibit strong distortions, presumably due to the formation of Re-Re metallic pairs along the $[ReO_6]_\infty$ octahedral chains. There are four sets of Cr-O distances ranging from 1.903(7) Å for Cr-O1 to 2.331(11) Å for Cr-O2, with an average $\langle Cr-O \rangle$ distance of 2.006(4) Å close to the ionic radii sum for Cr^{3+} (0.615 Å) and O^{2-} (1.40 Å). There are three sets of Re-O distances ranging from 1.83(5) Å for Re-O2 to 1.921(7) Å for Re-O3, with an average distance of 1.889(2) Å shorter than the ionic radii sum for Re^{5+} (0.58 Å) and O^{2-} (1.40 Å). The Cr-O1-Cr bond angles across the shared edge within the $[CrO_6]_\infty$ chains are the same and equal to 94.7(3)°; while the alternative short and long nearest-neighbor Re-Re

TABLE IV. Unit-cell parameters, Cartesian components of the Cr and Re magnetic moments, and agreement factors after the refinement of the magnetic structures of Cr_2ReO_6 and $CrReO_4$ from NPD data at 2 K.

	Cr_2ReO_6	$CrReO_4$
a (Å)	9.0798(2)	9.3256(2)
b (Å)	4.54095(2)	5.6564(1)
c (Å)	17.7583(3)	9.2376(2)
V(Å^3)	732.19(2)	486.98(1)
m_x(Cr)	0.37(9)	0.88(13)
m_y(Cr)	0.95(5)	0
m_z(Cr)	1.26(2)	1.72(8)
M (Cr)	1.63(4)	1.91(3)
m_x(Re)	−0.21(17)	0
m_y(Re)	0.03(8)	−0.30(7)
m_z(Re)	0.15(11)	0
M (Re)	0.26(19)	0.30 (7)
R_p(%)	6.14	5.96
R_{wp}(%)	8.95	7.94
R_{Bragg}(%)	5.42	8.25

TABLE V. Atomic coordinates and isotropic thermal factors B_{iso}[Å^2] for $CrReO_4$ from powder XRD data[a] at 295 K and the NPD data[b] at 120 K. Space group $C2/m$ (no. 12), $Z = 8$.

Atom	Site	T (K)	x	y	z	B_{iso}
Cr	4*i*	295	0.2435(6)	0.0	0.0040(13)	3.48(8)
		120	0.2513(12)	0.0	−0.0201(24)	0.82(9)
Re	4*h*	295	0.0	0.2745(2)	0.5	4.16(6)
		120	0.0	0.2641(10)	0.5	0.70(5)
O1	8*j*	295	0.3519(5)	0.2376(13)	0.2021(1)	2.7(1)
		120	0.3511(2)	0.2356(9)	0.2092(4)	0.11(4)
O2	4*i*	295	0.0664(9)	0.0	0.3473(23)	2.7(1)
		120	0.0969(8)	0.0	0.3086(12)	1.10(10)
O3	4*i*	295	0.6080(10)	0.0	0.2881(23)	2.7(1)
		120	0.6048(6)	0.0	0.2704(11)	0.43(9)

[a] $a = 9.3282(2)$ Å, $b = 5.6870(1)$ Å, $c = 4.6228(1)$ Å, $\beta = 92.065(1)^\circ$, $V = 245.08(1)$ Å^3. Discrepancy factors: $R_p = 3.23\%$, $R_{wp} = 4.83\%$, $R_{exp} = 2.59\%$, $\chi^2 = 3.48$, $R_{Bragg} = 5.79\%$.

[b] $a = 9.3429(2)$ Å, $b = 5.6767(2)$ Å, $c = 4.6255(1)$ Å, $\beta = 92.038(2)^\circ$, $V = 245.17(1)$ Å^3. Discrepancy factors: $R_p = 4.19\%$, $R_{wp} = 5.77\%$, $R_{exp} = 1.54\%$, $\chi^2 = 14.2$, $R_{Bragg} = 7.34\%$.

distances within the $[ReO_6]_\infty$ chains give rise to Re-O-Re bond angles of 83.8(1)° and 117.0(1)°, respectively. For those Cr-O-Re bonds connecting the $[CrO_6]_\infty$ and $[ReO_6]_\infty$ chains, the bond angles vary in the range between 121.4° and 138.1°.

Figure 7(a) shows the $\chi(T)$ of $CrReO_4$ measured under $\mu_0 H = 1$ T. Both ZFC and FC $\chi(T)$ curves overlap with each other and display a pronounced cusp anomaly at $T_N = 98$ K, signaling the occurrence of long-range AF order. The slight upturn at low temperatures should be attributed to the presence of a paramagnetic impurity. The inverse susceptibility $\chi^{-1}(T)$ shown in Fig. 7(b) also follows nicely the CW behavior in the paramagnetic region; a linear fitting was applied to obtain the $\mu_{eff} = 4.30(1)\mu_B$/f.u. and $\theta_{cw} = -478(1)$ K for $CrReO_4$. The obtained μ_{eff} is also smaller than the expected value of $4.8\mu_B$/f.u. for localized moments of Cr^{3+} ($g = 2$, $S = 3/2$) and Re^{5+} ($g = 2$, $S = 1$), similar to Cr_2ReO_6. The large negative θ_{cw} indicates a strong AF interaction. Interestingly, the large $f \equiv |\theta_{cw}/T_N| = 4.9$ signals the presence of considerable magnetic frustration in $CrReO_4$. Figure 7(c) shows the isothermal $M(H)$ curve of $CrReO_4$ at 2 K, which exhibits a nearly linear behavior in agreement with the AF order nature. The magnetization is very small, i.e., $0.036\mu_B$/f.u. at 7 T and

TABLE VI. Main interatomic distances (Å) and angles (°) of $CrReO_4$ from powder XRD data at 295 K.

Bond length (Å)					
CrO_6 octahedron			ReO_6 octahedron		
T (K)	295	120	T (K)	295	120
Cr-O1	1.903(7)	1.925(8)	Re-O1[e]	1.916(4)	1.900(2)
Cr-O1[a]	1.903(7)	1.925(8)	Re-O1[f]	1.916(4)	1.900(2)
Cr-O1[b]	1.966(7)	1.970(8)	Re-O2	1.831(5)	1.977(6)
Cr-O1[c]	1.966(7)	1.970(8)	Re-O2[g]	1.831(5)	1.977(6)
Cr-O2	2.331(11)	2.132(12)	Re-O3[h]	1.921(7)	1.988(6)
Cr-O3[d]	1.969(11)	1.806(12)	Re-O3[i]	1.921(7)	1.988(6)
⟨Cr-O⟩	2.006(4)	1.955(4)	⟨Re-O⟩	1.889(2)	1.955(2)
Cr-Cr[j]	2.846(2)	2.845(1)	Re-Re[o]	2.565(2)	2.678(8)
			Re-Re[m]	3.122(2)	2.998(8)
Cr-Re[k]	3.633(6)	3.534(10)	Cr-Re[m]	3.637(5)	3.534(10)
Cr-Re[l]	3.497(5)	3.51(1)	Cr-Re[n]	3.556(5)	3.534(10)
Bond angle (°)					
Cr-O1-Cr[j]	94.7(3)	93.82(2)	Re-O2-Re[m]	117.0(1)	98.64(1)
			Re[f]-O3-Re[p]	83.8(1)	84.67(1)
Cr-O1-Re[f]	132.6(3)	130.16(11)	Cr-O2-Re	121.4(2)	130.65(2)
Cr-O1-Re[k]	76.4(1)	78.01(6)	Cr[d]-O3-Re[f]	138.1(2)	137.28(1)

Symmetry transformations used to generate equivalent atoms:
[a] x, −y, z; [b] 0.5−x, −0.5+y, −z; [c] 0.5−x, 0.5−y, −z; [d] 1−x, y, −z; [e] −0.5+x, 0.5−y, z; [f] 0.5−x, 0.5−y, 1−z; [g] −x, y, 1−z; [h] 0.5−x, 0.5+y, 1−z; [i] −0.5+x, 0.5+y, z; [j] 0.5−x, 0.5+y, −z; [k] 0.5+x, 0.5−y, −1+z; [l] 0.5+x, 0.5−y, z; [m] −x, −y, 1−z; [n] −x, −y, −z; [o] −x, 1−y, 1−z; [p] 0.5+x, −0.5+y, z.

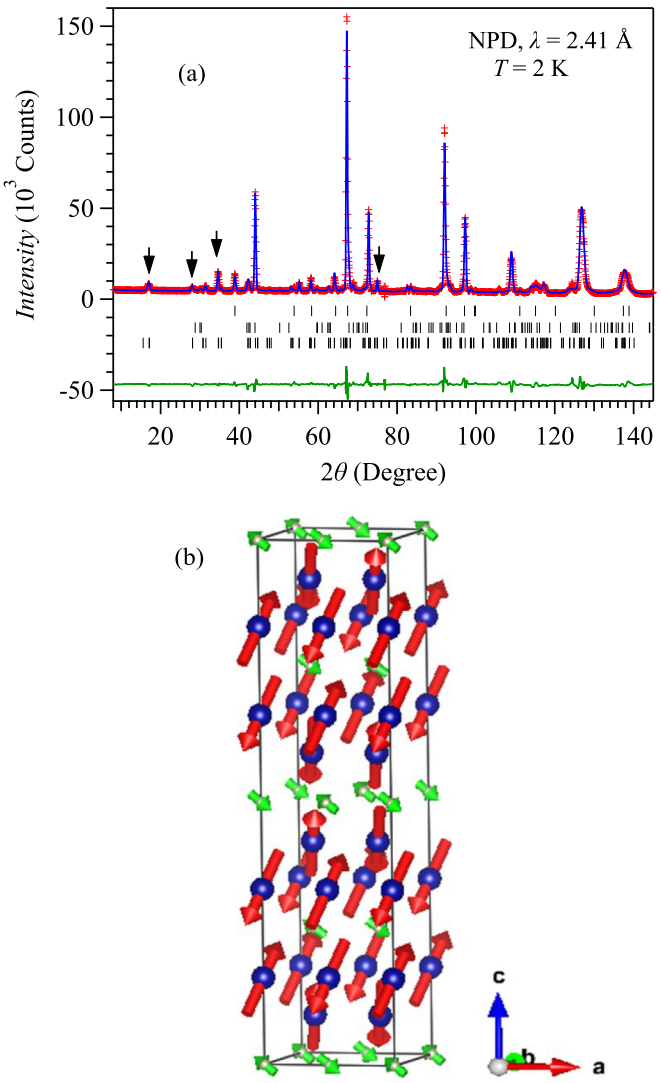

FIG. 4. (a) Observed (cross), calculated (line), and difference (bottom line) NPD profiles for Cr_2ReO_6 at 2 K. The first and second reflection marks correspond to the Cr_2O_3 and $CrReO_4$ minor impurities, and the third row belongs to the crystal and magnetic structure of Cr_2ReO_6. The magnetic reflections are indicated by the arrows. (b) The magnetic structure of Cr_2ReO_6 with the Cr moments (red) lying on the *bc* plane, and the small value of the Re moments (green) approximately lying on the *ac* plane.

2 K, implying a nearly perfect collinear AF arrangement of magnetic moments as confirmed below.

In a similar way, the additional reflections observed at 2 K for $CrReO_4$ could be indexed with a propagation vector $\mathbf{k} = [1,0,0.5]$. Using the MAXMAGN software, we also determined the maximal magnetic space groups for the parent space group $C2/m$ (no. 12) and the propagation vector $\mathbf{k} = [1,0,0.5]$ and analyzed the possible alternative models. The best fit was found for the magnetic subgroup C_c2/c. The coupling between different magnetic atoms in the structure is detailed in Table III. The goodness of the Rietveld fit at 2 K is illustrated in Fig. 8(a). A pure phase is identified in this case, and the magnetic reflections are indicated by the arrows.

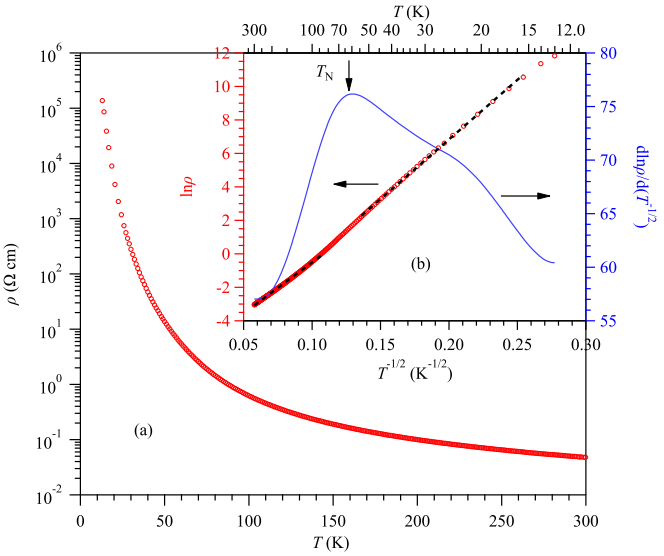

FIG. 5. (a) Temperature dependence of the resistivity $\rho(T)$ for Cr_2ReO_6. (b) A plot of $\ln\rho$ vs $T^{-1/2}$ showing an inflection point around T_N, which can be seen from the maximum of the $d\ln\rho/d(T^{-1/2})$ curve. The linear fitting curves shown by the dotted lines are used to extract the activation energies below and above T_N.

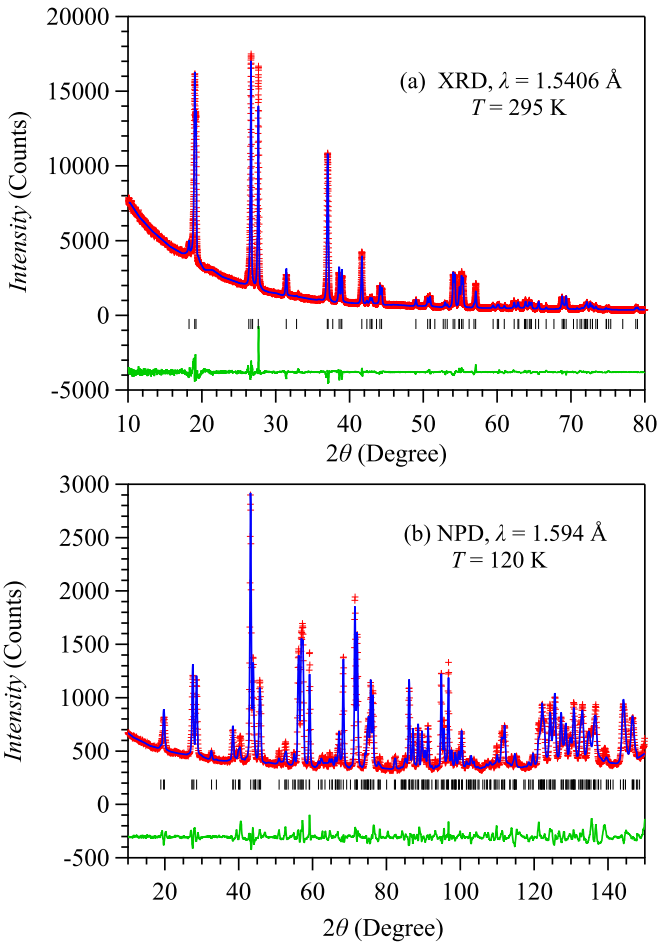

FIG. 6. Observed (cross), calculated (line), and their difference (bottom line) profiles of (a) XRD pattern at 295 K and (b) NPD pattern at 120 K for $CrReO_4$ after Rietveld refinements. The tick marks represent the Bragg positions of the birutile structure.

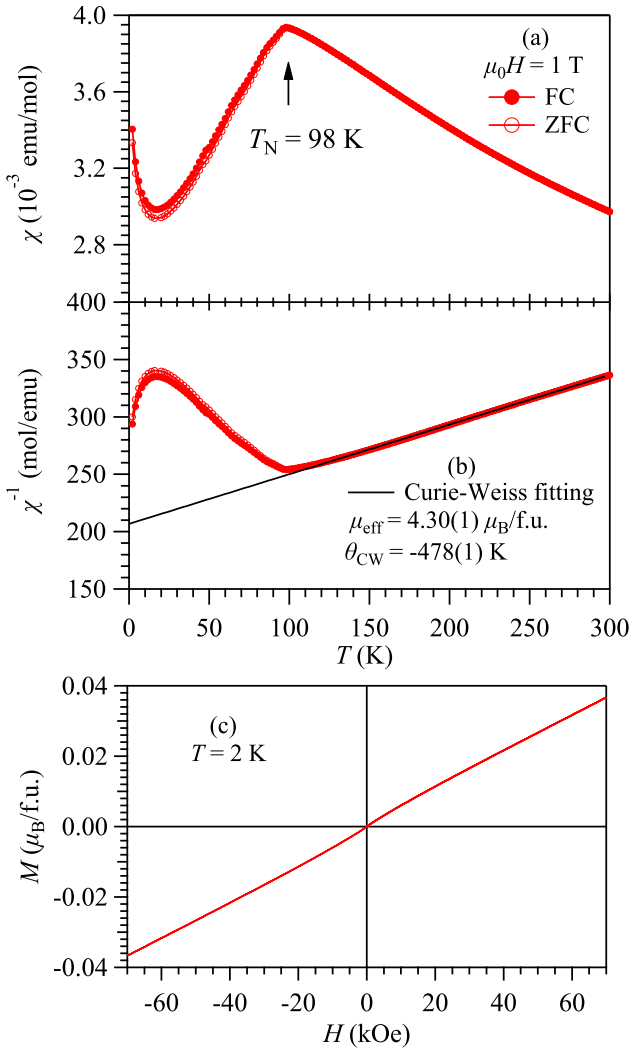

FIG. 7. Temperature dependence of (a) the magnetic susceptibility $\chi(T)$ and (b) its inverse $\chi^{-1}(T)$ for $CrReO_4$ measured in the zero-field-cooled (ZFC) and field-cooled (FC) modes. The Curie-Weiss fitting curve is shown by the solid line. (c) Field dependence of the isothermal magnetization $M(H)$ at 2 K.

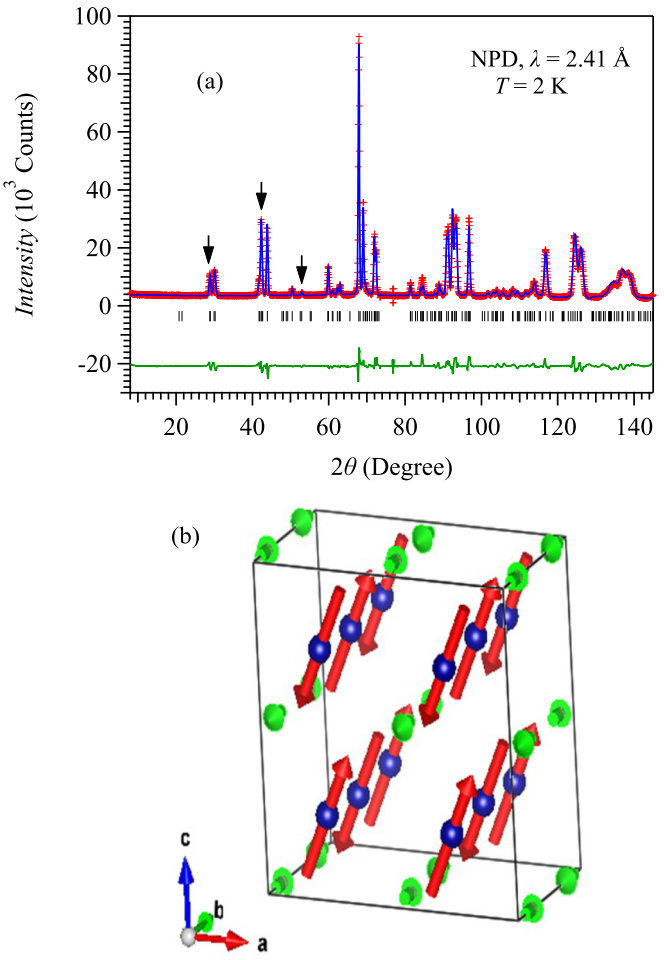

FIG. 8. (a) Observed (cross), calculated (line), and difference (bottom line) NPD profiles for $CrReO_4$ at 2 K. The series of vertical marks define the Bragg positions for both crystal and magnetic structures. The magnetic reflections are indicated by the arrows. (b) The magnetic structure of $CrReO_4$, showing the antiferromagnetic arrangement of the Cr moments (red) lying on the *ac* plane, and the tiny magnitude of the ordered Re moments (green) with a single component along the *b* axis.

The determined magnetic structure is displayed in Fig. 8(b). The ordered Cr magnetic moments lie in the *ac* plane, showing a perfect collinear AF structure that propagates along the *b* and *c* axes. The refined magnitude of the Cr magnetic moments is $1.91(3)\mu_B$, which is close to that obtained in Cr_2ReO_6. Similarly, the refined Re moment is also small, $\sim 0.3\mu_B$, pointing along the *b*-axis direction. The reduced moment of Re ion is presumably due to the spatially much more extended 5*d* orbitals. Table IV also contains the magnetic components of both Cr and Re moments for $CrReO_4$.

$CrReO_4$ also displays a semiconducting behavior in the whole temperature range. As shown in Fig. 9(a), its room-temperature resistivity is about 0.069 Ω cm and increases by five orders of magnitude upon cooling down to 2 K. In contrast with Cr_2ReO_6, the $\rho(T)$ of $CrReO_4$ can be better described by the three-dimensional VRH model, i.e., $\rho = \rho_0 \exp(T/T_0)^{-1/4}$, as shown in Fig. 9(b). Similarly, an anomaly can also be discerned around T_N in the derivative curve, implying a coupling of charge and spin degrees of freedom in this compound.

The presence of AF order and the semiconductor character for $CrReO_4$ is further supported by the specific heat $C(T)$ measurements. As shown in Fig. 10(a), a clear specific-heat anomaly is observed near 92 K, corresponding to the AF order seen in Fig. 7(a). The $C(T)$ data below 12 K are plotted in Fig. 10(b) in the form of C/T versus T^2. From the linear fitting shown as the solid line, we obtained a very small electronic Sommerfeld coefficient $\gamma = 1.62(3)\,\mathrm{mJ/mol\,K^2}$, in agreement with the semiconducting behavior. Since both lattice and AF order have a T^3 dependence at low temperatures, we cannot separate their contributions properly.

In order to estimate the magnetic contribution C_m associated with the AF order at high temperatures, we have simulated the lattice contribution C_{lat} from the $C(T)$ data above T_N by using one Debye and two Einstein components. As shown by the solid line in Fig. 10(a), the $C(T)$ data above T_N can be described

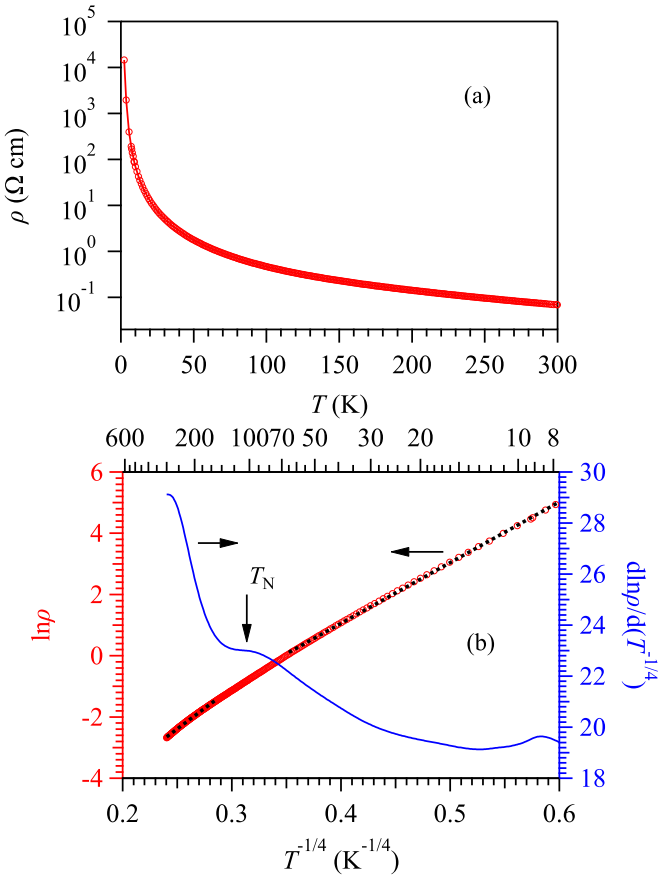

FIG. 9. (a) Temperature dependence of the resistivity $\rho(T)$ for $CrReO_4$. (b) A plot of $\ln\rho$ vs $T^{-1/4}$ showing a slope change around T_N, which can be seen from the plateau of the $d\ln\rho/d(T^{-1/4})$ curve. The linear fitting curves shown by the dotted lines are used to extract the activation energies below and above T_N.

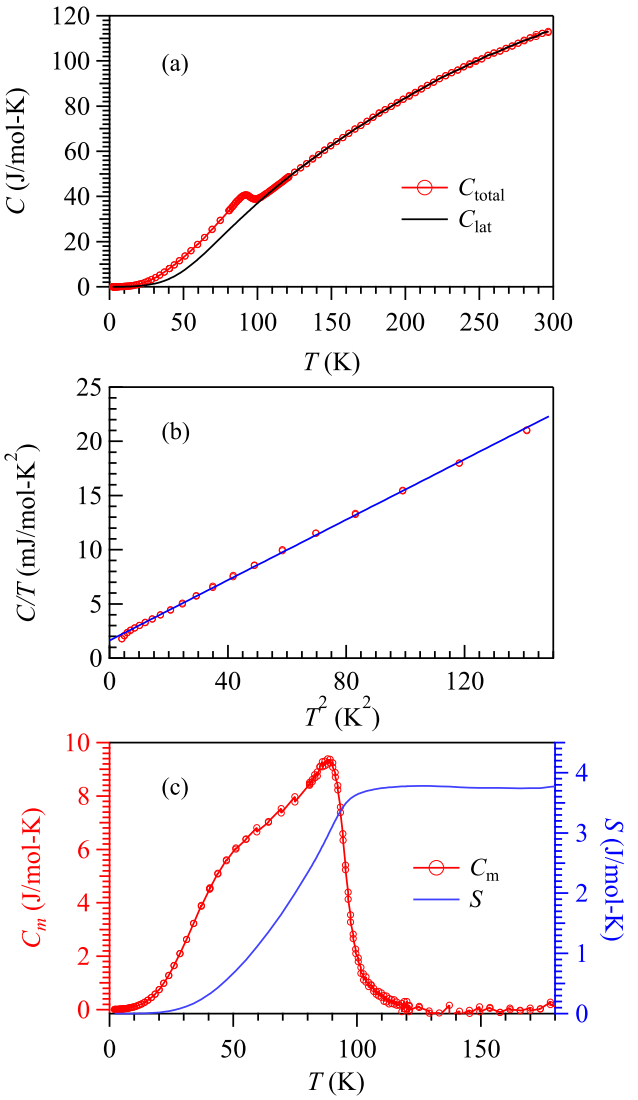

FIG. 10. (a) Temperature dependence of the specific heat $C(T)$ for $CrReO_4$. (b) The $C(T)$ data below 12 K in the form of C/T vs T^2. The solid line is a linear fitting curve. (c) The magnetic contribution $C_m(T)$ and the associated entropy $S(T)$ around T_N.

well by C_{lat}; the obtained Debye and Einstein temperatures are $\theta_D = 369$ K, $\theta_{E1} = 364$ K, and $\theta_{E2} = 926$ K, respectively. The obtained $C_m = C - C_{lat}$ and the associated magnetic entropy S obtained by integrating C_m/T over the investigated temperature range are displayed in Fig. 10(c). The cooperative AF order takes place below 100 K and seems to extend in a large temperature range. As can be seen, S reaches a constant value of 3.76 J mol^{-1} K^{-1}, which is much smaller than the expected value of 20.66 J mol^{-1} K^{-1} for localized Cr^{3+} ($S = 3/2$) and Re^{5+} ($S = 1$). There are several factors responsible for the large discrepancy between the observed and expected magnetic entropy: (i) the presence of magnetic frustration indicated by the large f factor should remove a considerable amount of magnetic entropy above T_N; (ii) the fitting to total $C(T)$ above T_N with the lattice contribution should underestimate the magnetic contribution; (iii) the polycrystalline nature of the sample broadens the AF transition; and (iv) the actual magnetic moments of both Cr^{3+} and Re^{5+} are smaller than expected, especially for Re^{5+}, according to the NPD results.

C. Discussion

Under moderate HPHT conditions, in the present study we have successfully obtained cation-ordered inverse trirutile Cr_2ReO_6 and monoclinic birutile $CrReO_4$ with sufficient phase purity for comprehensive physical property characterizations. There are several important factors for achieving this in comparison with the previous study [13]: (i) We performed the HPHT syntheses at about 1000 °C, which is about 200–400 °C lower than those used in Ref. [13]; a lower reaction temperature helps to maintain the high-valent Re^{6+} in Cr_2ReO_6. (ii) We employed a sealed Au capsule as the sample container, which can effectively prevent reactions with the surrounding materials and help to preserve the oxygen content. Instead, the hexagonal BN was used as the sample crucible in Ref. [13]. As a result, it not only reacts with the starting materials to form $CrBO_3$, but also produces a strong reducing atmosphere to stabilize $CrReO_4$ rather than Cr_2ReO_6.

Rietveld refinements on their XRD/NPD data confirmed a high degree of cation ordering in these two compounds due to the large difference of Cr/Re valence states, which can be calculated via the bond valence sum (BVS). The Brown bond

valence model gives a phenomenological relationship between the formal valence of a bond and the corresponding bond length [19,20]. The valence of Cr(Re) ions is the sum of individual bond valence $s_i = \exp[(d_0 - d_i)/D]$, in which $D = 0.370$ is a fixed value and d_0 is an empirical bond-valence parameter that varies for different valence states of a given cation [21]. For the nominal Cr^{3+} ion, the empirical value of $d_0 = 1.724$ was used for the Cr^{3+}-O^{2-} pair in the internal table of FULLPROF software. Based on the refined crystal structure information, the calculated BVS of Cr ion is 3.16(1) for Cr_2ReO_6 and 3.32(4) for $CrReO_4$, respectively. The calculated BVS for the Re ion in $CrReO_4$ is 4.67(2) based on the $d_0 = 1.860$ for the Re^{5+}-O^{2-} pair. Because there is no empirical value of d_0 for the Re^{6+}-O^{2-} pair in the internal table of FULLPROF software, we cannot obtain the BVS for Re ion in Cr_2ReO_6. These results confirmed that the actual valence states of cations in both compounds are close to the formal valence states.

A metallic behavior has been inferred in Ref. [13] from the nonzero electron density of states at the Fermi energy based on the X-ray photoelectron spectroscopy (XPS) valence spectra of mixed phase samples. But the XPS method probes the electronic structure at the surface region only. Here, bulk resistivity measurements confirm that both Cr_2ReO_6 and $CrReO_4$ are actually semiconductors following Mott's VRH conduction mechanism. Although the grain boundary effect in these polycrystalline samples could alter the exact temperature dependencies of resistivity, the relative small values of resistivity at room temperature, 0.048–0.069 Ω cm, for both compounds are consistent with a semiconducting nature. In these mixed-orbital systems, the charge carries participating in the VRH process should mainly come from the low-lying $Re^{6+/5+}(5t_{2g}^1/t_{2g}^2)$ orbitals with a large spatial extension, while the Cr^{3+} $(3t_{2g}^3)$ electrons are primarily localized. Since the Cr^{3+} and $Re^{6+/5+}$ are antiferromagnetically coupled, the hopping of Re-t_{2g} electron to the nearest-neighbor empty minority-spin Cr − t_{2g} orbitals should cost less energy than to the partially occupied majority Re-t_{2g} orbitals due to the on-site Coulombic repulsion. As a result, the hopping between Re^{5+} and Cr^{3+} should occur across the ReO_6 and CrO_6 octahedral chains in $CrReO_4$, leading to a VRH in three dimensions. On the other hand, the presence of edge-shared $[Cr_2ReO_{14}]_\infty$ chains in Cr_2ReO_6 renders a quasi-one-dimensional VRH as observed in Fig. 5. In addition, the hopping of Re-t_{2g} electrons to the empty minority-spin Cr-t_{2g} orbitals can rationalize the observed reduced magnetic moment of Cr^{3+} ions. First-principles calculations are needed to further verify the electronic structures for these compounds.

As mentioned above, three members of Cr^{3+}-based inverse trirutile oxides Cr_2BO_6 (B = Te, Mo, W) have been well studied. In these compounds, the counter B^{6+} cation contains either a completely filled (for Te : $4d^{10}$) or empty (for Mo : $4d^0$ and W : $5d^0$) d shell, which is nonmagnetic but can influence the magnetic properties of Cr sublattice via the orbital hybridizations. It has been known that both Cr_2TeO_6 and Cr_2WO_6 are AF insulators with the Néel temperature $T_N = 93$ and 45 K, respectively [6]. Interestingly, their detailed magnetic structures differ in a subtle way: the intrabilayer Cr^{3+} spins [see Fig. 1(c) for the crystal structure] are coupled antiferromagnetically for Cr_2TeO_6 but ferromagnetically for Cr_2WO_6 [6]. Given the similar ionic radii for nonmagnetic Te^{6+} and W^{6+} as well as the very similar Cr-O-Cr bond lengths and angles in these two compounds, the observed distinct magnetic structures cannot be rationalized within the framework of superexchange interactions based on the Goodenough-Kanamori rules. Aided by the first-principles electronic structure calculations, Zhu *et al.* [10] recently proposed that the sign and strength of the Cr-O-Cr superexchange interactions are strongly influenced by the hybridization between the O-2p and the empty W-5d orbitals; the virtual transfer of an O-2p electron to the empty W-5d orbital leads to an intrabilayer ferromagnetic coupling. Such a scenario was further elaborated in a latter study on Cr_2MoO_6 synthesized under HPHT conditions [11]. These studies underscore a different approach to tune the magnetic exchange interactions between Cr^{3+} ions in the trirutile structure via modifying the d-shell occupancy of the counter B^{6+} cation. In comparison with Cr_2BO_6 (B = Te, Mo, W), the presence of partially filled 5d orbital of Re^{6+} in Cr_2ReO_6 should introduce more complex magnetic interactions and stronger orbital hybridizations with oxygen. Thus, the availability of Cr_2ReO_6 offers an opportunity to shed further light on this interesting magnetic phenomenon.

The magnetic structure of Cr_2ReO_6 shown in Fig. 4(b) indeed differs from those of Cr_2TeO_6 and Cr_2WO_6. For the Cr^{3+} sublattice, both intra- and interbilayer Cr^{3+} spins in Cr_2ReO_6 are coupled antiferromagnetically, which is similar to that of Cr_2TeO_6, but the easy plane of the Cr^{3+} moments is different: the Cr^{3+} spins were found to lie in the ab basal plane for both Cr_2TeO_6 and Cr_2WO_6 [6], whereas they are tilted within the bc plane in Cr_2ReO_6. Since the Cr^{3+} (t_{2g}^3) should have a negligible anisotropy, such a difference should be attributed to the presence of partially filled 5d orbitals in the counter cation Re^{6+}. As seen in Fig. 4(b), the small Re^{6+} moments are coupled with each other antiferromagnetically within the ac plane, but the c-axis components are coupled ferromagnetically with the nearest-neighbor Cr moments along the c axis. Such a ferromagnetic coupling is expected for the direct exchange between the edge-shared CrO_6 $(3t_{2g}^3)$ and ReO_6 $(5t_{2g}^1)$ octahedra along the c axis. The spatially more extended 5d orbital might enhance this interaction. It is interesting to note that the magnetic moments of Cr and Re sublattices in Cr_2ReO_6 exhibit a noncollinear arrangement, with moments lying in the bc and ac planes, respectively, which is not commonly seen in other $3d - 5d$ coupled systems such as the double-perovskite A_2BOsO_6 (A = Ca, Sr; B = Fe, Co) [22,23]. Such a difference might arise from the fact that, in contrast with the perovskite structure, the Cr-O-Re bond angles in the rutile-type structure deviate significantly from 180° (see Table II). Indeed, a similar noncollinear alignment of the Cr and Re sublattices is also observed in $CrReO_4$, Fig. 8(b).

The observation of considerable frustration index $f = 4.9$ in $CrReO_4$ is also interesting. As a matter of fact, a similar situation has also been reported in isostructural compounds: $CrMoO_4$ ($T_N = 100$ K, $\theta_{cw} = -415$ K, and $|\theta_{cw}/T_N| = 4.15$) [24] and $CrWO_4$ ($T_N = 45$ K, $\theta_{cw} = -255$ K, and $|\theta_{cw}/T_N| = 5.67$) [9]. Since the rutile-type structure is not a typical geometrically frustrated lattice, the observation of a large f factor in these birutile compounds might have a common origin, presumably associated with the quasi-one-dimensional

character of the magnetic chains. Indeed, the magnetic susceptibility of $CrWO_4$ was found to display a broad hump at $T > T_N$ [9], which has been considered as characteristic of quasi-one-dimensional magnetic systems. Although such a hump feature is absent in Fig. 7(a) for $CrReO_4$, stronger intrachain interactions should render the system closer to a quasi-one-dimensional system and might be responsible for the large f factor.

IV. CONCLUSION

In summary, we have prepared the cation-ordered inverse trirutile Cr_2ReO_6 and monoclinic birutile $CrReO_4$ under moderate HPHT conditions, and performed detailed characterizations on their structural, transport, and magnetic properties. A second-order AF transition is found to take place at $T_N = 67$ K for Cr_2ReO_6 and $T_N = 98$ K for $CrReO_4$, respectively. Their magnetic structures were determined from the analysis of the NPD patterns. Both compounds are confirmed to display a semiconducting behavior following Mott's VRH conduction mechanism. A weak anomaly can be discerned around T_N from the temperature derivative of resistivity for both compounds, signaling a coupling between spin and charge degrees of freedom for these $3d-5d$ coupled electron systems.

ACKNOWLEDGMENTS

This work was supported by the CAS, NSFC, and MOST of China (Grants No. QYZDBSSW-SLH013, No. 11574377, No. 2014CB921500, No. XDB07020100). J.A.A. gratefully acknowledges the Spanish MINECO for granting the project MAT2013-41099-R.

[1] Y. Shimakawa, Inorg. Chem. **47**, 8562 (2008).
[2] Y. W. Long, N. Hayashi, T. Saito, M. Azuma, S. Muranaka, and Y. Shimakawa, Nature (London) **458**, 60 (2009).
[3] G. King and P. M. Woodward, J. Mater. Chem. **20**, 5785 (2010).
[4] M. W. Lufaso, Chem. Mater. **16**, 2148 (2004).
[5] G. Bayer, J. Am. Ceram. Soc. **43**, 495 (1960).
[6] W. Kunnamnn, S. L. Placa, L. M. Corliss, and J. M. Hastings, J. Phys. Chem. Solids **29**, 1359 (1968).
[7] A. Collomb, J. J. Capponi, M. Gondrand, and J. C. Jourbert, J. Solid State Chem. **23**, 315 (1978).
[8] C. Gleitzer, J. Less-Common Metals **51**, 215 (1977).
[9] J.-P. Doumerc, S. Angelov, F. Menil, and M. Pouchard, Mater. Res. Bull. **11**, 673 (1976).
[10] M. Zhu, D. Do, C. R. Dela Cruz, Z. L. Dun, H. D. Zhou, S. D. Mahanti, and X. Ke, Phys. Rev. Lett. **113**, 076406 (2014).
[11] M. Zhu, D. Do, C. R. Dela Cruz, Z. Dun, J.-G. Cheng, H. Goto, Y. Uwatoko, T. Zou, H. D. Zhou, S. D. Mahanti, and X. Ke, Phys. Rev. B **92**, 094419 (2015).
[12] A. W. Sleight, Inorg. Chem. **14**, 597 (1975).
[13] D. Mikhailova, H. Ehrenberg, D. Trots, G. Brey, S. Oswald, and H. Fuess, J. Solid State Chem. **182**, 1506 (2009).
[14] H. M. Rietveld, J. Appl. Crystallogr. **2**, 65 (1969).
[15] J. Rodriguez-Carvajal, Physica B **192**, 55 (1993).
[16] R. D. Shannon, Acta Crystallogr. A **32**, 751 (1976).
[17] J. M. Perez-Mato, S. V. Gallego, E. S. Tasci, L. Elcoro, G. de le Flor, and M. I. Aroyo, Annu. Rev. Mater. Res. **45**, 217 (2015).
[18] N. F. Mott, Philos. Mag. **19**, 835 (1969).
[19] N. E. Brese and M. O'Keeffe, Acta Crystallogr. B **47**, 192 (1991).
[20] I. D. Brown, Z. Kristallogr. **199**, 255 (1992).
[21] I. D. Brown and D. Altermatt, Acta Crystallogr. B **41**, 244 (1985).
[22] R. Morrow, K. Samanta, T. S. Dasgupta, J. Xiong, J. W. Freeland, D. Haskel, and P. M. Woodward, Chem. Mater. **28**, 3666 (2016).
[23] R. Morrow, J. W. Freeland, and P. M. Woodward, Inorg. Chem. **53**, 7983 (2014).
[24] Y. Shimony and L. Ben-Dor, Mater. Res. Bull. **15**, 227 (1980).